Ozone as oxidation agent in cyclic activation of biochar

Diana Jimenez-Cordero, Francisco Heras, Noelia Alonso-Morales, Miguel A. Gilarranz, Juan J. Rodriguez*

Universidad Autónoma de Madrid. S.D. Ingeniería Química. Ctra. Colmenar Viejo, km15. 28049. Madrid (Spain)

Corresponding author: Francisco Heras. Universidad Autónoma de Madrid. fran.heras@uam.es

Ph: +34914978051. Fax: +34914973516

Keywords: biochar, granular activated carbons, grape seed, activation, ozone

Abstract

Granular activated carbons were produced from grape seed biochar by cyclic activation with ozone. In each cycle, char was first oxidized by exposure to ozone and then subjected to high temperature in inert atmosphere to desorb oxygen groups formed. The study assessed the influence of operating conditions in the development of porosity, from a starting biochar with narrow microporosity (S_{BET}: 47 m^2g^{-1}, S_{DA}: 505 m^2g^{-1}) prepared by flash pyrolysis of grape seed at 800ºC. The variables studied were the number of cycles applied and the oxidation and desorption temperatures (250-275 and 850-950 ºC, respectively). High oxidation temperatures led to higher burn-off, which was also found to increase with the number of activation cycles. The burn-off needed to achieve a high surface area was lower than in conventional physical activation. After 7-9 activation cycles, activated carbons with S_{BET} higher than 1200 m^2g^{-1} and S_{DA} above 1500 m^2g^{-1} were obtained. The use of ozone resulted in mainly microporous activated carbons (0.37-

0.52 cm^3g^{-1}) with very low contribution of mesopores (<0.04-0.07 cm^3g^{-1}). The mean micropore size increased with the number of activation cycles due to pore widening, while mesopore mean size decreased along the cycles. The activated carbons showed a unique granular morphology with a hollow core and a porous shell, which is maintained even after 10 activation cycles.

1. Introduction

Agricultural residues have been widely studied for biochar and activated carbon preparation due to their low cost and the interest in the valorization of regionally-abundant resources [1,2]. Works in literature have reported on the preparation of activated carbons from different agricultural wastes [3-7]. Special interest has been paid to nut shells and hulls [3,8-14] and fruit stones [15-18].

Grape seed, whose production reaches about 15% of solid wastes generated during wine manufacturing, shows an interesting potential in terms of availability, morphology and chemical composition [13,19,20]. Previous works, focused on the use of grape seed as a starting material for activated carbon preparation using conventional activation, report BET specific surface area (S_{BET}) values around 400-500 m^2g^{-1} obtained at burn-offs around 75% by means of one-step pyrolysis/activation at 800ºC with steam [17]. Activation of grape seed with phosphoric acid at 500-550ºC resulted in S_{BET} values of up to 1140 m^2/g and important contribution of mesoporosity, while the initial granular morphology was preserved [21]. Physical activation with carbon dioxide resulted in mainly microporous materials (S_{BET} 700 m^2/g) with wide pore size distribution and low ash content [22].

In an earlier work by our group [18], grape seed biochar [20] was used as starting material in the preparation of activated carbon by cyclic activation using air (oxygen) as oxidizing

agent. Cyclic oxidation-desorption with oxygen has been proposed for a controlled activation, enabling the production of activated carbons with targeted porosity [18.23,24]. In the cyclic activation technique, each activation cycle is divided in two stages. Firstly, the starting material is subjected to low-temperature oxidation; secondly high-temperature desorption of chemisorbed oxygen is performed under inert atmosphere. Successive cycles are applied until the intended increase and/or modification of porosity is reached.

The application of activation cycles at different conditions leads to different porosity development patterns and surface chemical composition. The ability to tune the surface chemical composition is of great interest for numerous applications [25], but further research is needed to evaluate the feasibility of the preparation of activated carbons by cyclic activation, including the use of other gas-phase activating agents that can provide activated carbons with specific characteristics.

Former studies in literature have studied the effect of ozone oxidation on the development of porosity in carbon materials. Itoh et al. [26] reported effective oxidation of carbon at temperatures of up to 300ºC; maximum carbon oxidation rate is observed at temperatures around 250ºC, from that temperature, oxidation was found to decrease due to thermal decomposition of ozone. Álvarez et al. [27] reported on the degradation of the porous structure of commercial activated carbons when subjected to oxidation with gas phase ozone, showing that the modification increases with dose of ozone. A loss of S_{BET} and pore volume below 10% was observed when ozone-enriched air (40 mgL^{-1}) was used at 100ºC (12.7% burn-off). Belyaeva et al. [28] studied the modification of commercial granular activated carbons with 1.5% ozone in air at 25ºC. A short treatment time (1 h) led to a significant increase of S_{BET} (from 683 to 885 m^2g^{-1}) and total pore volume because of the “etching” of the surface of meso and macropores, which resulted in the formation

of new micropores. A more prolonged oxidation gave rise to destructive processes on the surface of micro and mesopores favoring their further broadening, together with partial blocking of pore mouths by ozonation products. Rivera-Utrilla and Sánchez-Polo [29] also observed a decrease in the surface area of commercial activated carbons when treated with ozone in gas phase at 25ºC for 20-120 min due to the ozone attack and the increase of oxygenated groups, these last preventing the diffusion of nitrogen during BET test by obstructing micropore entrances. Some works [19,20,27-30] also showed that ozone oxidation of carbon materials brings about a noticeable increase of the surface oxygen content due to the formation of oxygen-containing functional groups.

The results in literature show the ability of ozone to modify both the pore structure and chemical composition of carbon materials. The current work deals with the application of ozone in cyclic activation. The starting material is a biochar prepared by carbonization of grape seeds under optimized conditions [20] allowing to preserve the granular morphology of the seeds. This biochar shows a remarkable initial narrow microporosity that favors porosity development [18]. As in previous works in this research line, the aim is to learn on how to increase porosity at low burn-off values, thus preserving the initial morphology of the starting materials to achieve granular activated carbons with tailored porosity and surface chemical composition. The distinctive features of ozone as oxidant agent are also addressed.

2. Experimental

The starting char was prepared using residual grape seed generated in a local winery at the northwest of Spain. The crude material, water-washed and dried, was pre-treated by hexane extraction to remove oil, which is an important component of this kind of biomass [18]. In the current work 9% of the initial weight (dry basis) was removed as oil fraction.

The extracted grape seeds were subjected to flash pyrolysis at 800ºC, which was established as the optimum conditions in a previous work [18]. The biochar yield was 34 mass% (dry extracted seeds basis).

2.1. Samples characterization

The textural properties of the samples were determined from the isotherms of N_2 adsorption/desorption at 77 K and adsorption of CO_2 at 273 K, using a Micromeritics Tristar 2020 device. Prior to the analysis, the samples were degassed during 7 h at 150ºC using a VacPrep 061 degas accessory. BET, BJH and t-method were applied to calculate textural properties from N_2 isotherms, while Dubinin-Astakhov model was applied to calculate $S_{DA,}$ micropore volume and micropore mean size from CO_2 isotherms data [31]. In general terms, it can be considered that the specific surface area determined from CO_2 isotherms using Dubinin-Astakhov method (S_{DA}) gives information about the narrowest porosity (narrow microporosity), while the specific surface area determined from N_2 isotherm using BET method (S_{BET}) is mainly due to mesopores and wider micropores (around above 1nm in diameter). For that, the difference between S_{DA} and S_{BET} has been used throughout this paper as a useful indication of how much microporous is in a sample. The pore size distribution was characterized using the Non-Local Density Functional Theory (NLDFT) with pore geometry slit for both the CO_2 and N_2 isotherms [32].

A Quantachrome Poremaster 33 mercury porosimeter was used to characterize the meso-macroporous structure (50 – 100 nm interval) of the samples using the Washburn equation. The surface tension of mercury was taken as $4.8 \cdot 10^{-3}$ N·cm^{-1} and the mercury contact angle as 141º.

In cyclic activation, the type of surface oxygen groups generated during the oxidation stage is one of the variables affecting the development of porosity. In the current work,

the surface chemical groups of the activated carbons was characterized by Fourier Transform Infrared Spectroscopy (FTIR) using a Bruker IFS66v apparatus. The samples were mixed at 1 mass% with KBr for FTIR analysis.

The preservation of the initial granular morphology of the grape seeds is one the main features of the cyclic activation method studied. Changes in morphology were evaluated using a Hitachi S-3000N Scanning Electron Microscope (SEM).

2.2. Cyclic activation

The experimental procedures and devices used in this work for the cyclic activation of the biochar were those optimized in previous works [18,23,33]. The experimental set-up consisted on a vertical quartz-made electrical-heated reactor (45 cm length and 2.2 cm width). Ozone flow rate through the reactor during oxidation stage was 300 mgh^{-1}, and it was supplied by an electrical ozone generator from GMBOzone, model GMB-PRO-003. The generated ozone flow was further diluted in 50 $mLmin^{-1}$ of nitrogen. The desorption stage was carried out using only nitrogen and a flow rate of 100 $mLmin^{-1}$.

The activation conditions for the cycles were chosen according to a previous work [18]. The oxidation stage of each cycle was carried out at 250 and 275ºC for 2 h and the desorption step was performed at 850 and 950ºC under 100 $mLmin^{-1}$ nitrogen flow rate during 2 h. A heating rate of 10 $ºCmin^{-1}$ was use to switch from oxidation to desorption stage. The samples were labeled by the oxidation temperature, desorption temperature and the number of cycles applied, e.g. activated carbon 250-850C1 means 250 and 850ºC oxidation and desorption temperatures, respectively, and one activation cycle applied.

3. Results and Discussion

In cyclic activation, the porosity is modified mostly by thermal desorption, as CO and CO_2, of the surface functional groups generated during oxidation stage. As a general trend, a higher oxygen uptake results in a higher burn-off, causing higher porosity promotion per cycle, as it has been observed for air oxidation of biochars and waste tyre chars [18,33].

As can be observed in Figure 1, the variation of burn-off versus the number of cycles shows a linear profile for all the temperature combinations tested, with increments of 4.9–7.6 burn-off percentage points per cycle applied. Higher operation temperatures, both in oxidation and desorption stages, result in higher burn-off values. Thus, higher burn-off is achieved for the combination of temperatures 275/850 (oxidation/desorption, respectively).

Figure 1. Evolution of burn-off with activation cycles.

As shown in Figure 2, Type I isotherms (according IUPAC classification) were obtained for all the samples, which indicates the microporous structure of the activated carbons. Incipient H4-type hysteresis cycles that appear at relative pressure values above 0.3 indicate low contribution of mesoporosity. The starting biochar is characterized by a narrow microporosity, according to the large different between S_{DA} and S_{BET} values calculated for it (505 m^2g^{-1} and 47 m^2g^{-1}, respectively) [18]. Along the current work, the discussion is supported on both S_{BET} and S_{DA} values due to the heterogeneity of the

structure of the materials and their narrow microporosity, as it is the usual procedure in literature [31,34-39].

Figure 2. 77 K N_2 adsorption-desorption isotherms for the starting biochar and five-cycle activated carbons.

Figure 3 depicts the increase of surface area as consecutive activation cycles are applied. In general, a monotonic increase of S_{BET} (Figure 3a) was observed upon the successive cycles. For the series leading to the highest burn-off (275-850ºC) a much higher increase of S_{BET} was observed in the first cycle, which can be explained by both widening of previously existing narrow micropores and creation of new ones, since the S_{DA} also increased significantly in that first cycle. From the second activating cycle, widening of narrow micropores prevails, as shown by the decrease of S_{DA} accompanying the increase of S_{BET}. That combination of an oxidation temperature of 275ºC with a desorption temperature of 850ºC led to the highest burn-off and also allowed to achieve the highest surface area, reaching maximum values of S_{BET} of 1209 m^2g^{-1} (9^{th} cycle) and 1524 m^2g^{-1} for S_{DA} (7^{th} cycle). The difference between both surface area values indicates that narrow micropores can still be found in the samples due to their creation upon the successive cycles. This is a distinctive behavior of ozone as activating agent, as oxygen has been found to lead to the creation of new narrow micropores during cyclic activation in a much lower extent [18]. The lower generation of surface area during the last activation cycles can be partially ascribed to the formation of mesopores due to microporosity collapse by thermal stress, as proposed by Plyakov et al. [40]. Other authors [25,41] suggested that this phenomenon can be explained also by different effects of ozonation, such as

destruction of micropore walls and partial blockage of micropores by surface oxygen groups fixed on the pore entrance.

Figure 3. Evolution of S_{BET} (a) and S_{DA} (b) with activation cycles.

For a certain burn-off degree the generation of specific surface area depends on the activation conditions, especially during the earlier cycles. Thus, a higher effectiveness (surface area per burn-off unit) is observed when a desorption temperature of 950ºC was used. Similar combinations of S_{BET} and burn-off values can be obtained for all activated carbon series in the 600-800 m^2g^{-1} range, although the number of cycles needed to achieve such surface area development varies with the activation conditions.

Figure 4 shows the evolution of the S_{BET}/BO ratio versus number of cycles applied (a) and S_{BET} achieved (b), which can be interpreted as the change in surface area per mass percentage unit lost as a result of burn-off. Higher values of S_{BET}/BO ratio means that the porosity developed with smaller material loss. This figure confirms that the first activation cycles are more effective in terms of surface area generation per unit of burn-off. Such effectiveness decreases as more cycles are applied and a higher surface area is developed, even though the burn-off per cycle remains essentially constant, as shown in Figure 1. It must be taken into account that as the activated carbons develops S_{BET} resulting from micropores, additional burn-off leads in some extent to the collapse of micropore walls and therefore the generation of S_{BET} per unit of burn-off declines (Figure 4b). In Figure 4 it can also be seen that the factor that mostly affects the S_{BET} to burn-off ratio is the desorption temperature. Thus, a higher effectiveness in the development of porosity is

achieved through the combination of low oxidation and desorption temperatures, within the range tested.

Figure 4. Variation of S_{BET}/BO ratio with (a) activation cycles and (b) S_{BET}.

The evolution of micro and mesopore volume with the number of cycles, plotted in Figure 5, indicates that different patterns can be achieved in the development textural properties. In all cases a low mesopore volume was obtained (below 0.04-0.07 cm^3g^{-1}), whereas a marked increase of microporosity ocurred from the first activation cycle. It is relevant that the narrow (2-8 nm) and wide (8–50 nm) mesoporosity were only developed in some extent (> 0.005 cm^3g^{-1}) after the third-fourth cycle, which is consistent with the above mentioned destruction of micropores to form mesopores [42]. Mesopore generation became noticeable when micropore volume in the carbon was higher than 0.25 cm^3g^{-1}. After 10 activation cycles the material with the largest micropore volume (0.52 cm^3g^{-1}) showed a mesopore volume of almost 0.07 cm^3g^{-1}. The so well marked transition observed between micro and mesoporosity generation makes possible tayloring the type of porosity by an appropiate selection of the activation conditions and the number of cycles applied.

The generation of micropores during ozone cyclic activation is related to a lower oxidation rate compared to conventional gasification, which enables diffusion of the oxidant creation of surface oxygen groups even within micropores and leads to controlled widening of micropores. Likewise, the oxidation is carried out at conditions that minimize simultaneous uncontrolled gasification. In conventional activation the high temperature

used results in higher gasification rate, with increased gasification at the particle surface or pore mouths, even under chemical control conditions.

Figure 5. Micro and mesopore volume development with number of activation cycles.

The widening of existing micropores is also revealed by the increase of micropore mean size with the activation cycles, as shown in Figure 6a. The highest micropore mean size was obtained for the combination of 275 and 850 ºC oxidation and desorption temperatures (respectively). Likewise, Figure 6b shows that higher micropore mean size values were obtained at higher values of burn-off. With regard to the evolution of the mesopore mean size, a decrease can be observed with both number of cycles and burn-off (Figures 6c and 6d).

Figure 6. Micropore and mesopore mean sizes vs number of cycles (a and c) and burn-off (b and d).

The pore size distribution (PSD) is a vital issue regarding the characterization of porous carbons. One of the most used methods is based on the NLDFT [31]. NLDFT method was applied to calculate the micropore size distribution from CO_2 isotherms and the micro and mesopore size distribution from N_2 isotherms. Figure 7 shows the results for some selected samples with similar specific surface area (S_{BET} = 750-850 m^2g^{-1}) and burn-off (40% aprox.). As can be observed from CO_2 DFT distribution, the microporosity for all of these selected samples shows the same multi-modal microporosity distribution with three peaks at 0.45, 0.55 and 0.88nm. This profile was also observed in the initial biochar

[20], although the microporosity below 0.6–0.7 nm was higher for the biochar than for the activated samples. Some differences among samples can be observed for N_2 NLDFT distribution in the 1-3 nm pore size interval. The development of porosity in this range is negligible for the biochar, while the activated carbons show an important contribution of narrow mesoporosity centered at 2.2 nm. Among the activated samples, the differences are much less marked, but the pore volume in this range is slightly higher for the samples activated using 850ºC as desorption temperature. No significant contribution of porosity is observed between 4 and 20 nm, except an minor contribution at 8–10 nm for the initial biochar.

Figure 7. Pore size distribution by DFT method from CO_2 and N_2 isotherms for selected samples.

Figure 8 shows the results of macropore volume determination by mercury intrusion porosimetry for the activated carbons subjected to 1, 4, 7 and 10 activation cycles. The general trend of macropore volume is to increase with the activation cycles and hence with the burn-off. Very low differences can be observed in relation to operating conditions. The main increase of macroporosity is obtained from the cycle number 4.

Figure 8. Macropore volume (0.05-4μm pore size) from mercury intrusion porosimetry for all series evaluated versus (a) number of cycles and (b) burn-off.

The whole meso and macropore size distributions obtained by mercury porosimetry (0.01-4μm), shown in Figure 9, indicate that similar distributions are obtained for all

samples. However, higher pore volumes were generated for an oxidation temperature of 275ºC combined with a desorption temperature of 950ºC, particularly in the case of macropores.

Figure 9. Macropore and mesopore size distribution between 0.01 and 4μm for samples after 10 activation cycles.

Figure 10 shows the FTIR spectra of the char and the activated carbons after the fifth cycle of oxidation-desorption. FTIR analysis cannot be considered as quantitative characterization, but it is widely accepted for semi-quantitative evaluation of the changes in carbon surface chemistry. The results obtained are quite similar to those obtained in previous works using air as oxidation agent [18], indicating that surface functional groups formation occurs by similar mechanisms for both oxygen and ozone. All spectra show similar profiles but different intensities. The spectra exhibit three main broad bands centered at 1070, 1500 and 3400 cm^{-1}. In general, a higher absorption intensity can be observed for the samples prepared at a desorption temperature of 850ºC, except for the band around 1070 cm^{-1}, whose intensity is higher for samples oxidized at 275ºC. In this wavenumber range the presence of oxygen groups is shown by the overlapping of bands in the 1300 to 900 cm^{-1} range, where γ(O—H) vibrations in ring ethers and primary C—O single bond stretching vibration from γ and δ lactone groups, aromatic and aliphatic ether, and epoxide structures occur [27].

The overlapping of absorption bands in the 1400-1700 cm^{-1} range are mainly due to the olefinic γ(C=C) vibrations, ν(C=C) stretching vibration and skeletal C=C vibrations in aromatic rings of some surface oxygen groups such as lactones and quinones. For the

samples obtained at a oxidation temperature of 275ºC is particularly significant the higher absorption of the peak c.a. 1625 cm^{-1}, which can be associated to olefinic ν(C=C) vibrations and aromatic skeletal stretching. For all the samples, the peak observed at 3600-3650 cm^{-1} is due to the stretching of O-H bonds of water that constitutes the moisture taken for the KBr during sample preparation for FTIR analysis. At around 1600 cm^{-1} can be observed a much less intense adsorption corresponding to the bending of these bonds. Moreover, in this region can be found the adsorption of ν(O—H) and γ(O—H) vibrations in phenolic hydroxyl groups associated by hydrogen bonds [26]. It is remarkable that even when the highest desorption temperature is used, not all functional groups are desorbed from the carbon surface; some of them can be considered as heat resistant and hence not relevant to porosity development. However, as they scale-up on the carbon surface the reactivity of the surface may be lower.

Figure 10. FTIR spectra of grape seed char and samples after 5 activation cycles.

In Figure 11 the results of S_{BET} vs. burn-off obtained in this work are compared to those found in literature for the activation of biomass agricultural by-products such as apricot and cherry stones [13], olive stones [1], pecan shells [3], coconut shells [6] and other biomass wastes activated with steam [1,4,5,8,9,13,14] and CO_2 [1,6,9-12,14,43] by conventional physical activation. It can be observed that the activated carbons obtained from grape seeds biochar by ozone cyclic activation show comparatively high S_{BET}/BO ratios.

Figure 11. Comparison of S_{BET} vs. burn-off values obtained by ozone cyclic activation and by other methods from literature.

The SEM images of the starting biochar and the activated samples (Figure 12) indicate that no important morphological changes were induced by the ozone treatment and the desorption at high temperature. The initial seeds shape is kept along the activation process, even after 10 cycles due to the controlled burn-off.

Figure 12. SEM micrographs of (a) char from grape seeds and activated carbons (b) 275-850 C5 and (c) 275-850 C10.

As can be seen in Figure 13 the pyrolysis led to a volatilization of the endosperm material leaving a low density structure in the inner portion of the char granules. Such low density layer is also found in the activated sample. It can also be seen that most of the mass of the activated carbon granules is allocated in the periphery. This structure can be of interest regarding potential applications implying mass transfer phenomena since the material combines granular morphology and a short diffusion path, with a thickness of the outer layer around 200 μm.

Figure 13. SEM images of different sections of samples: cross section (a) and wall detail (b) of activated sample after 10 activation cycles at 275/850 oxidation/desorption temperatures; cross section (c) and outer layer detail (d) of initial grape seed biochar.

4. Conclusions

The use of ozone as oxidation agent in the cyclic activation of biochar from waste grape seed has been assessed. The method offers good control of the activation conditions and generation of surface area at low burn-off, thus keeping the initial granular shape of the biochar particles.

The variation of burn-off with number of cycles shows a linear trend. The highest values of burn-off were obtained for the activated carbons prepared at 275ºC and 850ºC oxidation and desorption temperature, respectively. These conditions also led to the highest values of S_{BET}. A steady increase of S_{DA} was observed, which indicates the creation of new micropores during al the activation procedure. Some development of of macroporosity was also observed during the activation.

Ozone cyclic activation led to essentially microporous activated carbons, with very low contribution of mesopores. The content of surface oxygen groups in the activated carbons increased with the number of activation cycles, indicating that the desorption stage does not remove all the oxygen incorporated during the oxidation.

5. Acknowledgment.

The authors greatly appreciate financial support from the Spanish Ministerio de Ciencia e Innovación (CTQ2012-32821).

6. References

[1] El-Sheikh A.H., Newman A.P., Al-Daffaee H.K., Phull S., Cresswell N. *J. Anal. Appl. Pyrolysis.* **2004**, 71, 151-164.

[2] Ioannidou O., Zabaniotou A. *Sustain. Energy Rev*. **2007**, 11, 1966-2005.

[3] Ahmedna M., Marshall W.E., Rao R.M. *Bioresour. Technol*. **2000**, 71, 113-123.

[4] El-Hendawy A-NA., Samra S.E., Girgis B.S. *Colloids Surf A Physicochem. Eng. Asp*. 180 (2001) 209-221.

[5] Fan M., Marshall W., Daugaard D., Brown R.C. *Bioresour. Technol*. **2004**, 3, 103-107.

[6] Guo S., Peng J., Li W., Yang K., Zhang L., Zhang S., Xia H. *Appl. Surf. Sci.* **2009**, 225, 8443-8449.

[7] Tsai W.T., Chang C.Y., Lee S.L. *Bioresour. Technol*. **1998**, 64, 211-217.

[8] Ahmedna M., Marshall W.E., Husseiny A.A., Rao R.M., Goktepe I. *Water Res*. **2004**, 38, 1062-1068.

[9] Girgis B.S., Yunis S.S., Soliman A.M. *Mater. Lett*. **2002**, 57, 164-172.

[10] Iniesta E., Sánchez F., García A.N., Marcilla A. *J. Anal. Appl. Pyrolysis* **2001**, 58, 967-981.

[11] Lua A.C., Yang T., Guo J. *J. Anal. Appl. Pyrolysis* **2004**, 72, 279-287.

[12] Marcilla A., Garcia-Garcia S., Asensio M., Conesa J.A. *Carbon* **2000**, 38, 429 – 440.

[13] Savova D., Apak E., Ekinci E., Yardim F., Petrov N., Budinova T., Razvigorova M., Minkova V. *Biomass Bioenergy* **2001**, 21, 133-142.

[14] Wartelle L.H., Marshall W.E., Toles C.A., Johns M.M. *J. Chromatogr. A* **2000**, 879, 169-175.

[15] Gergova K., Petrov N., Eser S. *Carbon* **1994**, 32, 693-702.

[16] Gómez-Serrano V., Álvarez P.M., Jaramillo J., Beltrán F.J. *Thermal effects. Carbon* **2002**, 40, 513-522.

[17] Nakagawa Y., Molina Sabio M., Rodríguez Reinoso F. *Microporous Mesoporous Mater*. **2007**, 103, 29-34.

[18] Jiménez-Cordero D., Heras F., Alonso-Morales N., Gilarranz M.A., Rodríguez J.J. *Chem. Eng. J.* **2013**, 231, 172-181.

[19] Luque-Rodríguez J.M., Luque de Castro M.D., Pérez-Juan P. *Talanta* **2005**, 68, 126-130.

[20] Jiménez-Cordero D., Heras F., Alonso-Morales N., Gilarranz M.A., Rodríguez J.J. *Biomass Bioenergy* **2013**, 54, 123-132.

[21] Al Bahri M., Calvo L., Gilarranz M.A., Rodriguez J.J. *Chem Eng J*. **2012**, 203, 348-356.

[22] Bahri M., Calvo L., Gilarranz M.A., Rodriguez J.J. *Chem Eng Comm.* (acepted) DOI: 10.1080/00986445.2014.934447).

[23] Heras F., Alonso-Morales N., Jiménez-Cordero D., Gilarranz M.A., Rodríguez J.J. *Ind. Eng. Chem. Res*. **2012**, 51, 2609-2614.

[24] Py X., Guillot A., Cagnon B. *Carbon* **2003**, 41, 1533.

[25] Solís-Fernández P., Paredes J.I., Cosío A., Martínez-Alonso A., Tascón J.M.D. *J. Colloid Interface Sci.* **2010**, 344, 451-459.

[26] Itoh Y., Sakakibara Y., Shinjoh H. *RSC Adv*. **2014**, 4, 19144-19149.

[27] Álvarez P.M., García-Araya J.F., Beltrán F.J., Masa F.J., Medina F. *J. Colloid Interface Sci*. **2005**, 283, 503-512.

[28] Belyaeva O.V., Krasnova T.A., Semenova S.A. *Russian J. Appl. Chem.* **2011**, 84, 597-601.

[29] Rivera-Utrilla J., Sánchez-Polo M. *Adsorption* **2011**, 17, 611-620.

[30] Krawczyk P. *Chem. Eng. J.* **2011**, 172, 1096-1102.

[31] Gil A., Grange P. *Colloids Surf A Physicochem. Eng. Asp.* **1996**, 113, 39-50.

[32] Jagiello J., Thommes M. *Carbon* **2004**, 42, 1227-1232.

[33] Heras F., Alonso N., Gilarranz M.A., Rodríguez J.J. *Ind. Eng. Chem. Res*. **2009**, 48, 4664-4670.

[34] Carrasco-Marin M., Lopez-Ramon M.V., Moreno-Castilla C. *Langmuir* **1993**, 9, 2758-2760.

[35] Dubinin M.M. *Carbon* **1981**, 19, 321-324.

[36] Gil A., Montes M. *Langmuir* **1994**, 10, 291-297.

[37] Jaroniec M., Choma J. *Mater. Chem. Phys* **1988**, 19, 267-289.

[38] Jaroniec M., Gilpin R.K., Kaneko K. *Langmuir* **1991**, 7, 2719-2722.

[39] Rodwadowski M., Wojsz R. *Carbon* **1984**, 22, 363-367.

[40] Polyakov M., Poisot M., Maurits W.E., Drescher T., Lotnik A., Kienle L., Bensch W., Muhler M., Grunert W. *Catal. Commun*. **2010**, 12, 231-237.

[41] Sing K.S.W., Everett D.H., Haul R.A.W., Moscou L., Pierotti R.A., Rouquerol J., Siemieniewska T. *Pure Appl. Chem*. **1985**, 57, 603.

[42] Mysyk R., Gao Q., Raymundo-Piñero E., Béguin F. *Carbon* **2012**, 50, 3367-3374.

[43] Girgis B.S., Soliman Ashraf M., Fathy Nady A. *Microporous Mesoporous Mater*. **2011**, 142, 518-525.

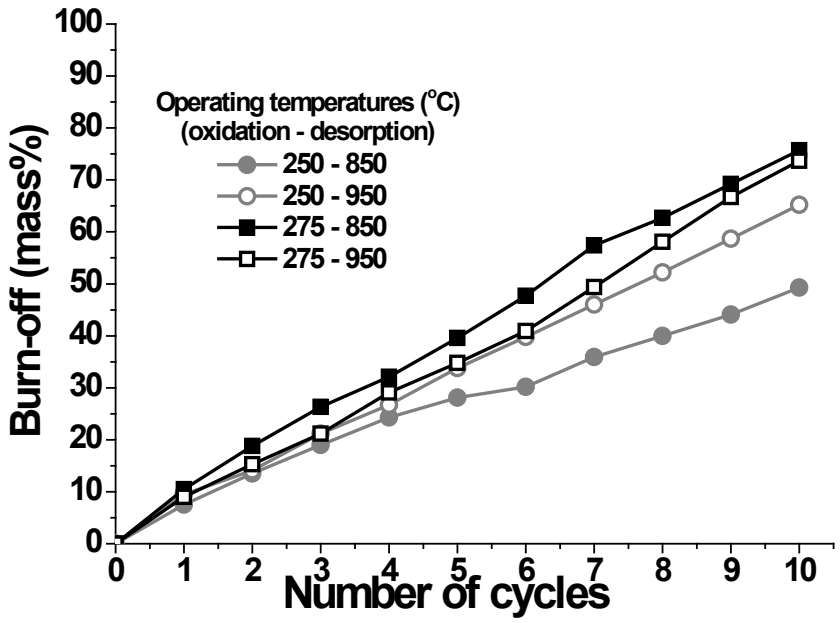

Figure 1. Evolution of burn-off with activation cycles.

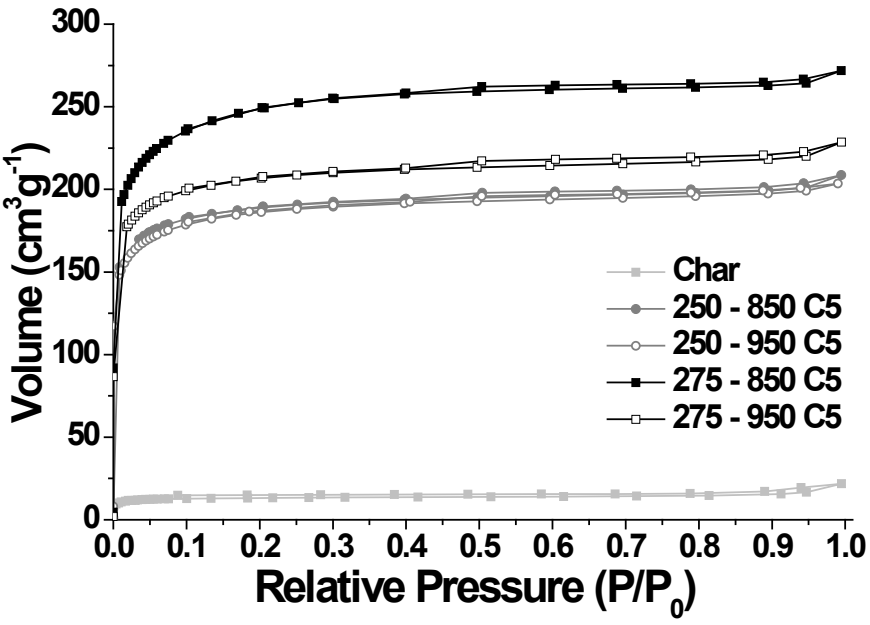

Figure 2. 77 K N_2 adsorption-desorption isotherms for the starting biochar and five-cycle activated carbons.

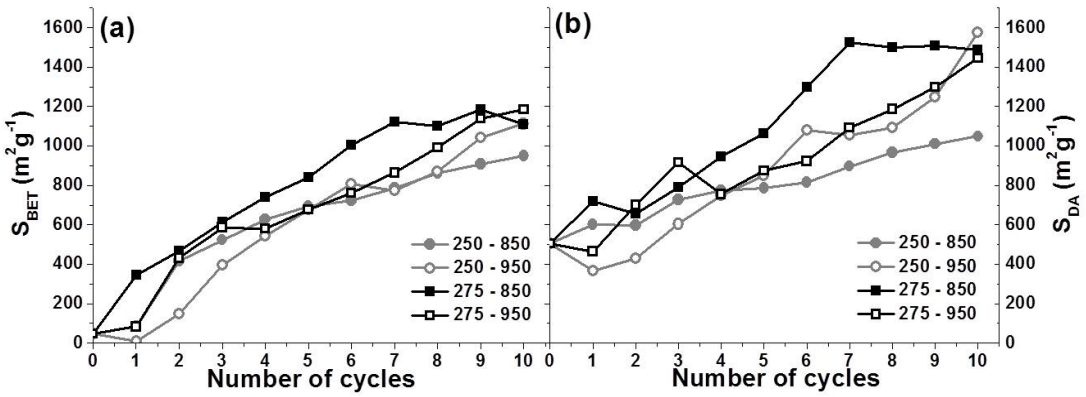

Figure 3. Evolution of S_{BET} (a) and S_{DA} (b) with activation cycles.

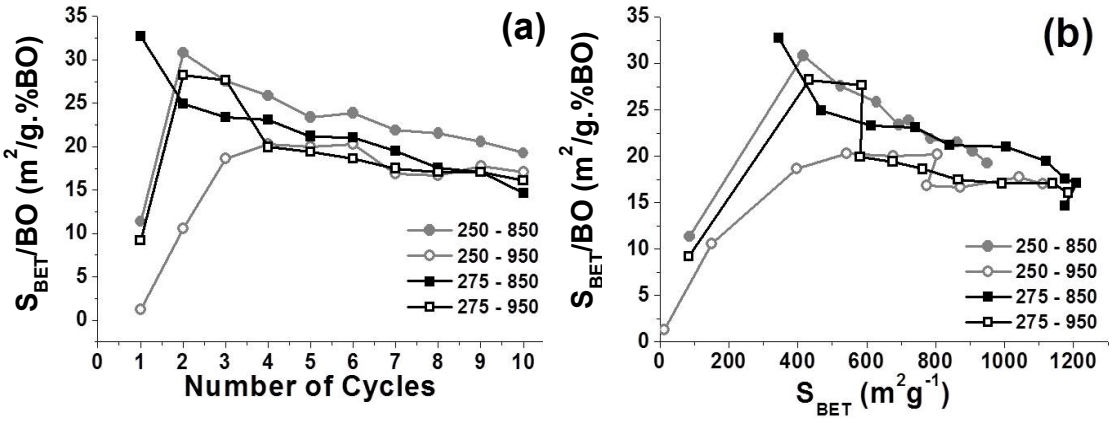

Figure 4. Variation of S_{BET}/BO ratio with (a) activation cycles and (b) S_{BET}.

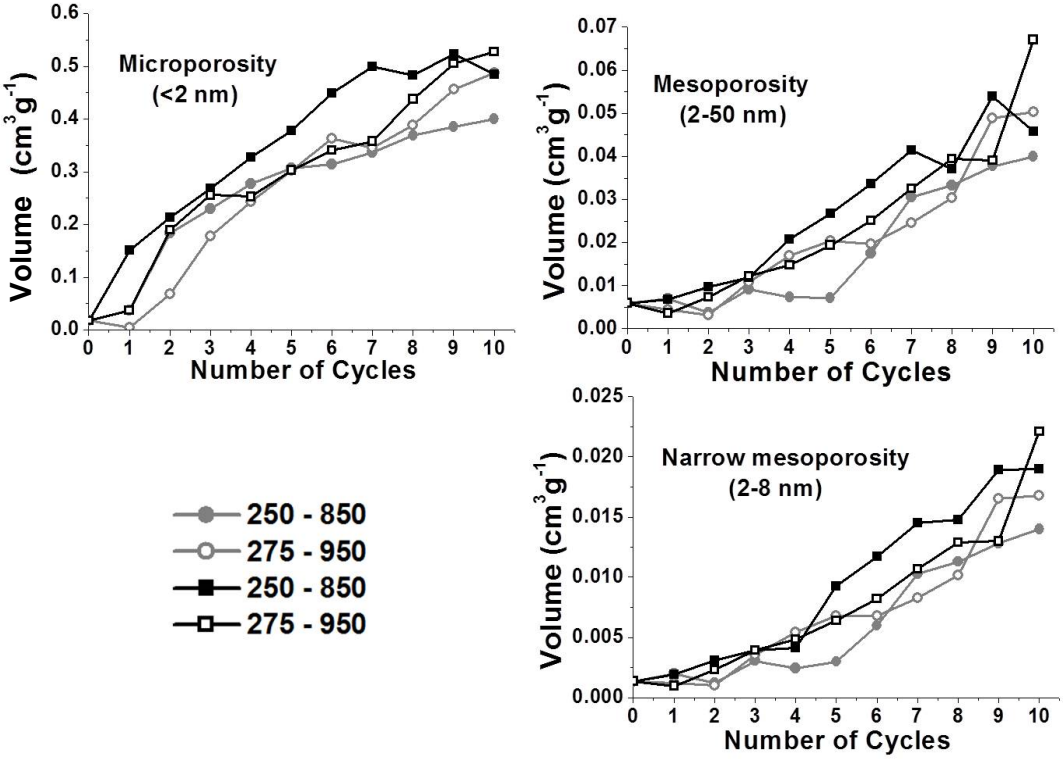

Figure 5. Micro and mesopore volume development with number of activation cycles.

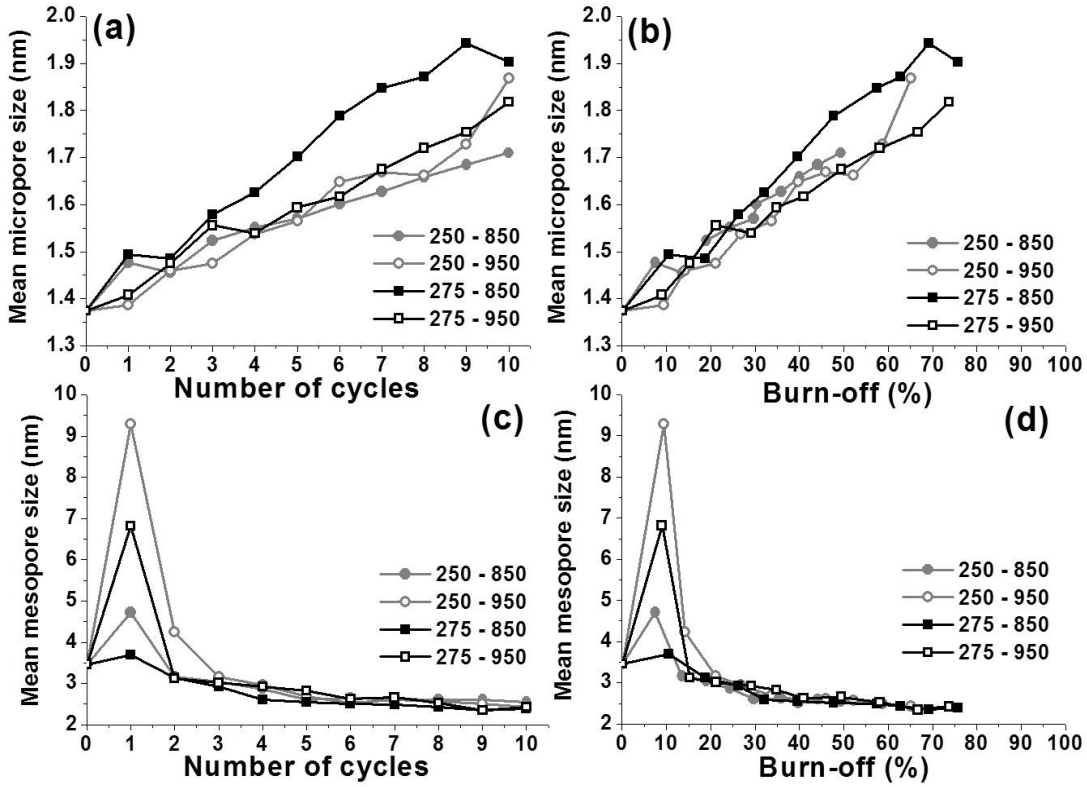

Figure 6. Micropore and mesopore mean sizes vs number of cycles (a and c) and burn-off (b and d).

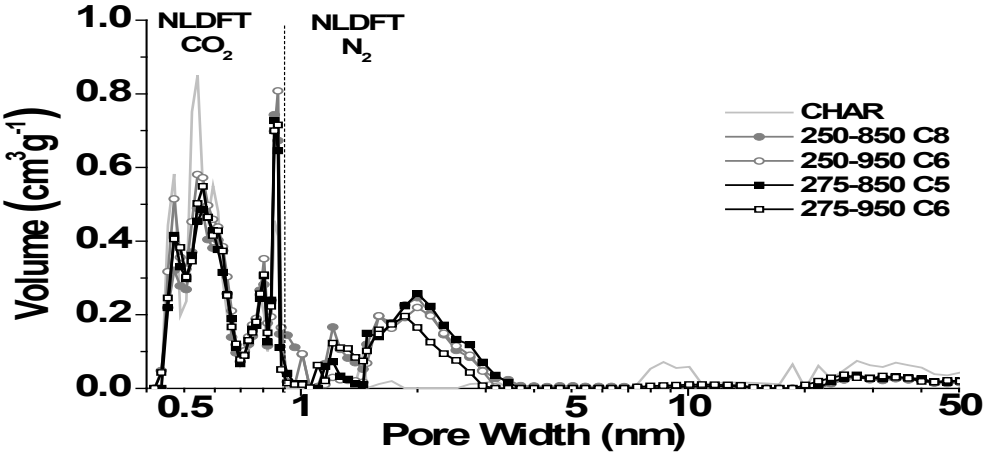

Figure 7. Pore size distribution by DFT method from CO_2 and N_2 isotherms for selected samples.

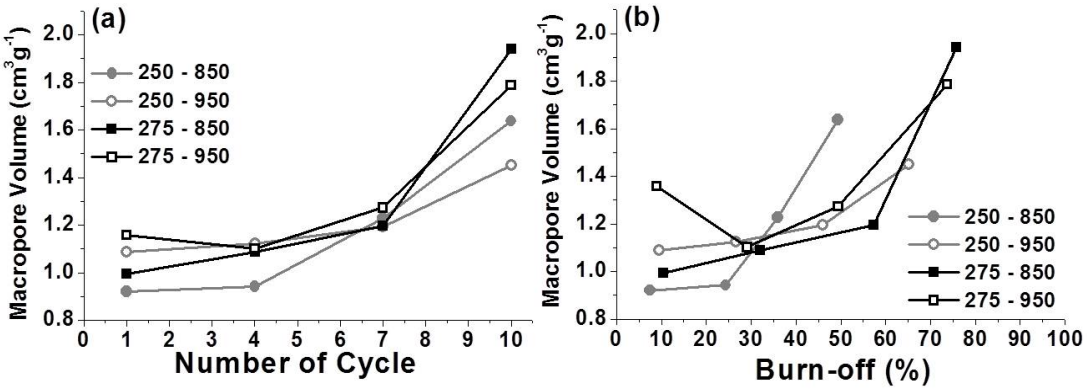

Figure 8. Macropore volume (0.05-4μm pore size) from mercury intrusion porosimetry for all series evaluated versus (a) number of cycles and (b) burn-off.

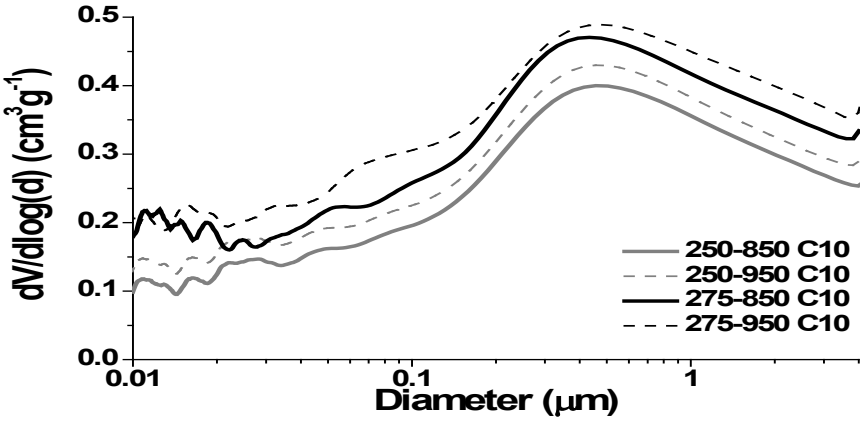

Figure 9. Macropore and mesopore size distribution between 0.01 and 4μm for samples after 10 activation cycles.

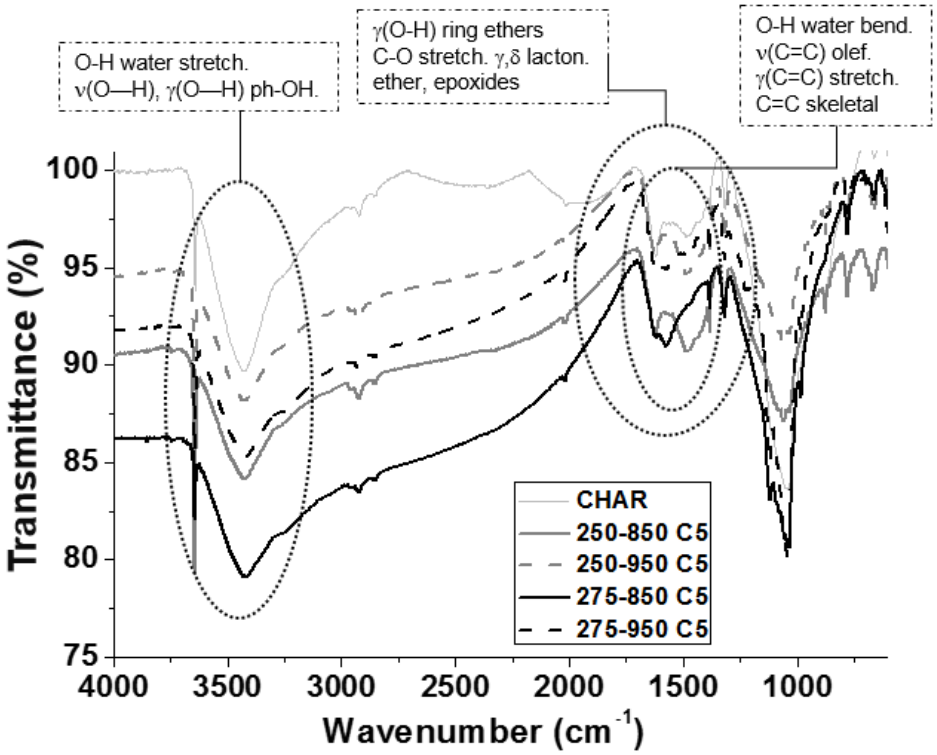

Figure 10. FTIR spectra of grape seed char and samples after 5 activation cycles.

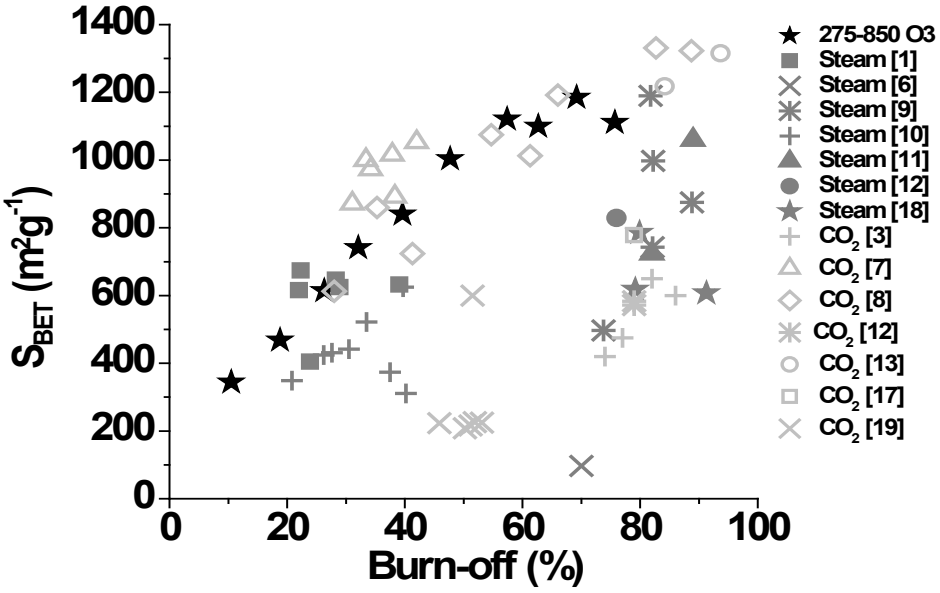

Figure 11. Comparison of S_{BET} vs. burn-off values obtained by ozone cyclic activation and by other methods from literature.

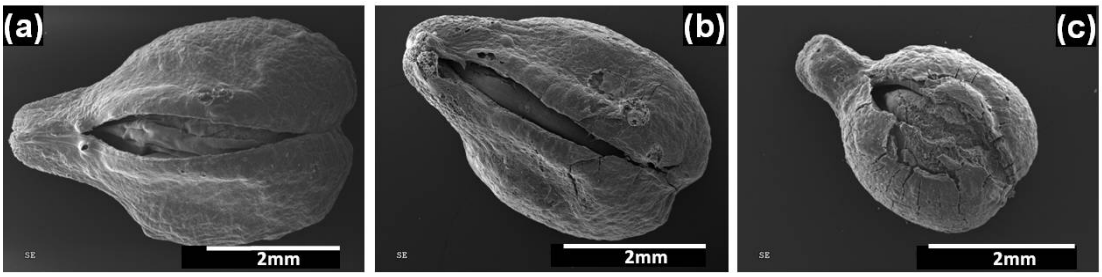

Figure 12. SEM micrographs of (a) char from grape seeds and activated carbons (b) 275-850 C5 and (c) 275-850 C10.

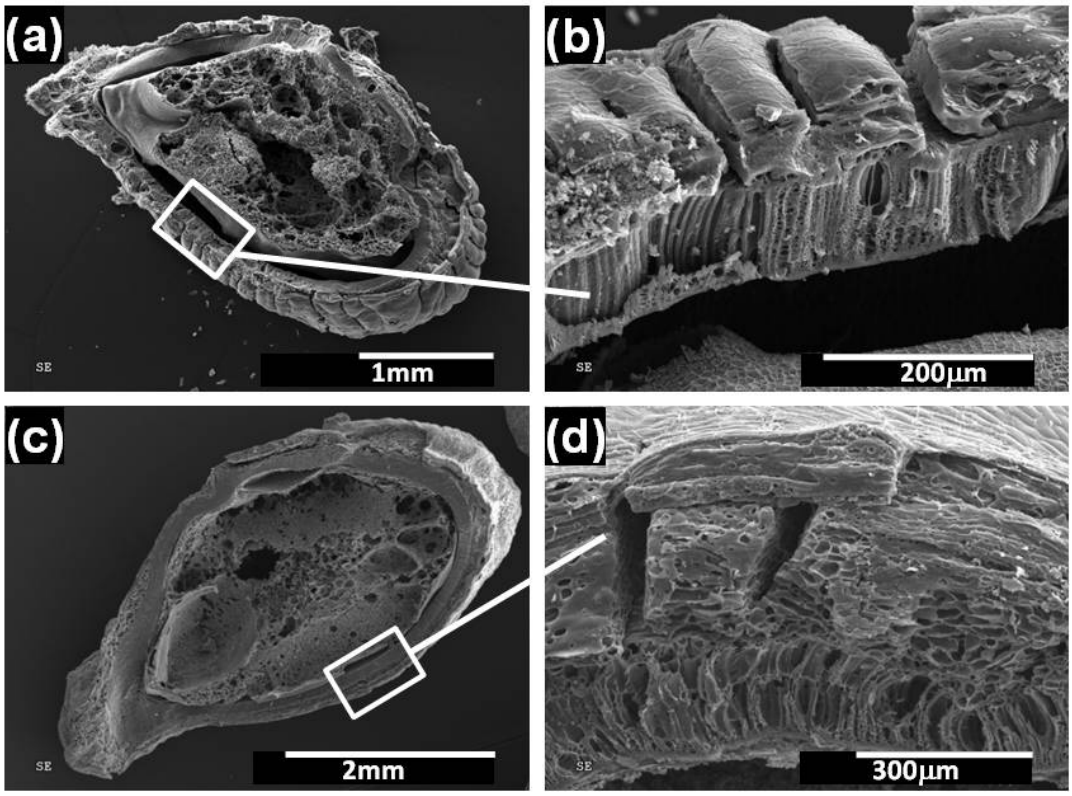

Figure 13. SEM images of different sections of samples: cross section (a) and wall detail (b) of activated sample after 10 activation cycles at 275/850 oxidation/desorption temperatures; cross section (c) and outer layer detail (d) of initial grape seed biochar.